Eclipse Spectropolarimetry of the ε Aurigae System

Kathleen M. Geise
Robert E. Stencel
University of Denver, Department of Physics and Astronomy, 2112 E. *Wesley Avenue, Denver, CO 80208; address email correspondence to kgeise@du.edu*

Nadine Manset
Canada-France-Hawaii Telescope Corporation (CFHT), Waimea Headquarters, 65-1238 Mamalahoa Highway, Kamuela, HI 96743

David Harrington
Jeffrey Kuhn
Institute for Astronomy, University of Hawaii, 2680 Woodlawn Drive, Honolulu, HI 96822

Received April 13, 2012; revised August 27, 2012, October 17, 2012; accepted November 4, 2012

Abstract The recent eclipse of the enigmatic binary star system, ε Aurigae, offered a special opportunity to explore the role of spectropolarimetry in discovery of unknown facets of the objects involved. Here we present spectropolarimetric results for H-alpha, H-beta, Ca I (422.6 nm), and K I (769.9 nm) based on more than 50 epochs of high dispersion spectra obtained with the ESPaDOnS instrument at CFHT during 2006–2012.

1. Introduction

The target, ε Aur, is a single line spectroscopic binary that features an opaque disk, surrounding a hidden companion, that causes a lengthy eclipse every 27 years—for a reading list, see, for example, Stencel *et al.* (2011). Instrumentation advances of the past decade have enabled a remarkable set of new spectropolarimetric data to be obtained during the 2008–2011 eclipse. The ESPaDOnS instrument (Donati 2003) at the Canada-France-Hawaii Telescope obtained more than 50 epochs of full Stokes polarimetry from 3800Å to 10000Å. Prior efforts have revealed broadband polarization changes during eclipses, successfully predicting some disk characteristics, as well as demonstrating post-eclipse variability (Kemp *et al.* 1986; Cole 2012). Spectropolarimetric observations may contribute to our understanding of the system by revealing the nature and distribution of gaseous material in the F-star atmosphere and in the occulting disk. This paper provides a description of data analyzed to date. Our preliminary results indicate that the increased polarization observed in broadband during eclipse is also present in many spectrographic lines.

2. Observations

The data were obtained using the EPSaDOnS instrument at the Canada-France-Hawaii telescope (CFHT). ESPaDOnS is a cross-dispersed échelle spectropolarimeter designed to obtain a complete optical spectrum in a single exposure, with a resolving power of about 70,000. The ε Aur data used in this report were obtained with about 10^6 counts per spectral bin. The normalized intensity (normalized to 1) corresponds to an average uncertainty of about 1×10^{-3}, for a signal-to-noise (S/N) of c. 1000. All four Stokes parameters were taken for each observation (see Table 1 for a log of observations).

We retrieved ESPaDOnS observations of ε Aur from the Canadian Astronomy Data Centre (CADC), CFHT Science Data Archive (http://www1.cadc-ccda.hia-iha.nrc-cnrc.gc.ca/cadc/). Fifty epochs of spectropolarimetric observations of ε Aur span the time from pre-eclipse (beginning February 2006) through the eclipse phases and include post-eclipse observations (for example, January 2012). The data were automatically reduced with Upena, CFHT's reduction pipeline for ESPaDOnS. Upena uses LIBRE_ESPRIT, which is a proprietary data reduction software tool (Donati *et al.* 1997).

2.1. Contributions of polarimetry to the study of ε Aur

Polarization signatures occur when symmetries are broken. Possible sources of polarization are rotation deformities, aspherical winds, tidal distortions in binary systems, the Chandrasekhar effect during eclipse of binary systems, photospheric inhomogeneities including radiation inhomogeneities, and matter streams or accretion. Polarization signatures due to scattering depend upon the nature and distribution of the scatterers: electrons, atomic species, and/or dust grains. Broadband polarization signatures (for example, see Cole 2012; Henson *et al.* 2012; Kemp *et al.* 1986; Coyne 1972) may include contributions from both the continuum and lines that may involve different scattering agents.

The spectropolarimetric observations included in this paper reveal anisotropies in gaseous atomic species intrinsic to the F star, as well as geometric and/or scattering effects of the disk during eclipse. One possible geometric source of polarization in lines during eclipse is the Chandrasekhar effect associated with limb polarization of the F star. One possible source of polarization out-of-eclipse is anisotropy associated with stellar pulsation, for example. Our goal is to identify the source or sources of polarization in the lines both in- an out-of-eclipse revealed by these excellent ESPaDOnS high-resolution observations. ESPaDOnS observations cannot be used to measure continuum polarization (http://www.cfht.hawaii.edu/Instruments/Spectroscopy/Espadons/).

3. Method

Linear polarization, P, was computed using normalized Q and U (that is, Q/I_c and U/I_c) for each wavelength in the observation according to Equation (1) (Bagnulo *et al.* 2009).

$$\frac{P}{I_c} = \sqrt{\left(\frac{Q}{I_c}\right)^2 + \left(\frac{U}{I_c}\right)^2} \tag{1}$$

Percent linear polarization was calculated as follows

$$\%\, p = \frac{P / I_c}{I / I_c} \times 100 \tag{2}$$

Where I/I_c denotes the normalized intensity. Percent q (%q), percent u (%u). and percent v (%v), where q, u, and v are the normalized Stokes parameters, were calculated in a manner similar to Equation (2).

Assessing the true errors in polarimetric measurements is crucial to establishing the physics of the source. We assume that the Stokes parameters Q and U are normally distributed about their true values, but it has been shown that linear polarization follows a Rice distribution (for example, Clarke and Stewart 1986). The Rice probability distribution is given by

$$\mathrm{R}(p \mid p_0, \sigma) = \frac{p}{\sigma^2} \exp\left[\frac{-p^2 + p_0^2}{2\sigma^2}\right] I_0\left(\frac{p p_0}{\sigma^2}\right) \tag{3}$$

Here p_0 is the underlying, true, polarization, I_0 is the zeroth-order modified Bessel function, and the underlying Gaussian noise has variance σ^2. In the limit of high signal-to-noise (S/N), the Rice distribution approaches the normal distribution, with a mean that approaches p_0 and a standard deviation that approaches σ (Vaillancourt 2006). The Rice mean is given by

$$\mu_R = \sqrt{\frac{\pi}{2}}\, \sigma\, L_{1/2}\left(\frac{-\mu^2}{2\sigma^2}\right) \tag{4}$$

Here $L_{1/2}(x)$ is a Laguerre polynomial of order ½, μ is the mean, and σ is the standard deviation. The Rice variance is given by

$$\frac{1}{2}\, \pi\sigma^2\, L_{1/2}^2\left(\frac{-\mu^2}{2\sigma^2}\right) \tag{5}$$

Here $L_{1/2}^2(x)$ is a generalized Laguerre polynomial $L_n^{(\alpha)}(x)$ with n = ½ and $\alpha = 2$. The Rice standard deviation may be found by taking the square root of the variance.

By definition, the parameter p is a positive definite quantity. The individual polarization values calculated from Equation (1) will always be positive and non-zero because the individual values of Q and U will generally be non-zero. At large S/N ($p/\sigma \geq 4$) the maximum likelihood and most probable estimators for the linear polarization (for example, Simmons and Stewart 1985) converge to

$$\hat{p} = \sqrt{(p^2 - \sigma^2)} \tag{6}$$

Equation (6) corrects for the positive bias in the linear polarization calculated using Equation (1) (Clarke 2010). The data presented here are not corrected for interstellar polarization.

The mean value of p may be computed using the mean values of q and u (Clarke and Stewart, 1986) as follows

$$\overline{p} = \sqrt{(\overline{q}^2 + \overline{u}^2)} \tag{7}$$

The barred variables denote the mean.

Linear polarization position angle, Θ, may be computed from Stokes q and u as follows (Bagnulo *et al.* 2009). Position angles will range from 0 to 180 degrees.

$$\Theta = \frac{1}{2}\, tan^{-1}\left(\frac{u}{q}\right) + \Theta_0 \tag{8}$$

$$\Theta_0 = \left\{ \begin{array}{c} 0 \text{ if } q > 0 \text{ and } u \geq 0 \\ 180 \text{ if } q > 0 \text{ and } u < 0 \\ 90 \text{ if } q < 0 \end{array} \right\}$$

$$\Theta = \left\{ \begin{array}{c} 45 \text{ if } q = 0 \text{ and } u > 0 \\ 135 \text{ if } q = 0 \text{ and } u < 0 \end{array} \right\} \tag{9}$$

The ESPaDOnS data are noisier at shorter wavelengths (that is, toward the blue) than longer wavelengths because the detector is less sensitive in the blue. We binned the linear polarization data with a wavelength bin of 0.015 nm using the error-weighted mean (for example, Taylor 1997) to boost signal-to-noise at shorter wavelengths and for deep absorption lines. We determined through trial and error that this was the largest bin size that did not seriously degrade the resolution of the line. In some cases, we combined several epochs (using the error-weighted mean) to further reduce noise prior to wavelength binning, using the criterion that the line profile did not change between binned epochs.

We computed the mean for both q and u using the binned data and then computed the mean linear polarization using Equation (7). The Rice mean and

variance were computed for each p using Equations (4) and (5), adopting the mean polarization for μ in those equations. Finally, we bias-corrected the linear polarization using Equation (6), adopting the Rice standard deviation for σ in that equation. We adopted the error bars given in the pipeline reduction as the uncertainty in both normalized intensity and normalized Stokes parameters and propagated those uncertainties in calculations of percent Stokes (see, for example, error bars in Figure 2). We also propagated the uncertainty (Rice standard deviation) in the calculation of %p (see, for example, error bars in Figure 1).

For polarizations with large S/N, the confidence regions approach those given by a normal Gaussian distribution centered on the bias-corrected value of p, with 2σ corresponding to 95% and 2.6σ corresponding to 99% confidence for $p/\sigma \geq 4$ (Vaillancourt 2006). The maximum likelihood estimator (Equation 6) of the underlying ("true") polarization converges with all other estimators when p/σ is greater than 4. For p/σ greater than 3 and less than 4, the maximum likelihood estimator may not completely correct for bias; the polarization is considered the upper bound. Values of p/σ less than 1.4 correspond to zero polarization (Vaillancourt 2006). We identified spectroscopic regions with significant linear polarization by flagging polarization peaks for $p/\sigma \geq 4$.

We rotated the unbinned data by 27 degrees using a rotation matrix (for example, Code and Whitney 1995; Bagnulo *et al.* 2009) to align instrument north with the rotation axis of the system as described by Kloppenborg *et al.* (2010) before binning by epoch and wavelength. We confirmed that the invariant, $(Q^2 + U^2)$, was conserved under rotation (intensity is unaffected by rotation and %p is unaffected as long as the invariant is conserved).

We verified that the null parameters provided by the ESPaDOnS pipeline contained no signal, indicating that any instrument effects were removed by the data reduction. We were also careful to change the sign of Stokes U as directed by the ESPaDOnS FITS file headers.

4. Analysis

4.1. Linear polarization time series and qu-plots

Initial analysis focused on the stronger lines in order to assess whether the eclipse resulted in changes to the polarization. A sample time-series of H-alpha line profiles and polarizations are shown in Figure 1. A sample plot of %q vs. %u (a qu-plot) is shown in Figure 2. The error bars in the qu-plot are the 1σ-propagated (assumed Gaussian) average uncertainties in both %q and %u. The angle from the +q axis measured counterclockwise to a feature in the qu-plot corresponds to twice the position angle (2Θ) as measured east of north and may be a useful diagnostic of the geometry of the scattering giving rise to the polarization. We were careful to exclude %q and %u contributions from neighboring lines in these plots when possible.

4.2. Hydrogen alpha

We fit the pre-eclipse H-alpha line (rest wavelength 656.280 nm) with a Gaussian function and adopted the HWHM of the Gaussian (c. 25 km s^{-1}) as the line core. We further defined the wings as follows: the blue wing (–125 km s^{-1} to –25 km s^{-1}) and the red wing (25 km s^{-1} to 125 km s^{-1}). Regions outside of these defined areas consistently mapped to (0,0) in the qu-plots. These definitions are maintained throughout the following analysis.

H-alpha exhibited persistent polarization in the line core in all epochs (see Figure 1). During pre-eclipse, the line core accounted for a nearly linear excursion of (–%u, –%q) in the qu-plot (green diamond symbol, Figure 2). The line was largely symmetric, with both red and blue emission wings evident. The line appeared slightly broadened to the red when compared to the Gaussian function. The blue and red emission wings exhibited no polarization features in this binned epoch, or in any pre-eclipse epoch. At no phase did the H-alpha line reach zero intensity.

Harrington and Kuhn (2009) noted the strong presence of spectropolarimetric signatures in and around the absorptive components of the H-alpha emission line in Herbig Ae/Be stars that they called "polarization-in-absorption." They also identified a broad polarization signature across emission features for many classical Be stars in their sample. Herbig Ae/Be stars are embedded in cold gas and dust, which may be equatorially enhanced, whereas classical Be stars are rapid rotators characterized by ionized equatorial material. The equatorial material surrounding these two types of stars contributes to distinctly different polarization signatures. The polarization features we observed in pre-eclipse ε Aur spectra are similar to "polarization-in-absorption"; this suggests that ε Aur does not have an equatorial enhancement of ionized material.

At mid-eclipse, and for many epochs following mid-eclipse, the line exhibited a central emission feature (presumed recombination, see Stencel *et al.* 2011). %p increased, consistent with changes to broadband polarization reported by Cole (2012) and Kemp *et al.* (1986). The core polarization peak appears notched in these epochs, possibly indicating a depolarization associated with the emission core. At mid-eclipse, the blue and red absorption wings exhibited broad %p polarization. There were excursions in the qu-plot for features in the line core (–%q; green diamond symbol), as well as the blue (+%q, +%u; blue square symbol) and red (+%q, –%u; red triangle symbol) absorption wings (Figure 2). These qu-plot excursions were not affected by binning and are evident in several observations around this time.

By late eclipse, the line exhibited a broad, deep, blue-shifted absorption. Normalized intensity dropped to about 10% at the deepest part of the line, but signal-to-noise remained above 700 and the ratio p/σ ranged from 3 to 25 for polarization greater than 0.4%, significant within the Rice statistics. The central core polarization remained strong (>1%) in late eclipse, but the blue wing polarization increased (>0.5% at –100 km s^{-1}), while the red wing polarization

decreased (that is, negligible at 100 km s^{-1}). In the qu-plot, the line core accounted for the –%q features (green diamonds), the blue wing accounted for the +%q features (blue squares), and the red wing polarization (red triangles) was largely concentrated at (0,0) (Figure 2). Thus, the polarization behavior followed the line behavior in this epoch.

The H-alpha line did not return to its pre-eclipse form by the time of our last post-eclipse observation (January 17, 2012). The red emission wing reappeared at about the pre-eclipse level, but the blue emission wing was masked by a broad (> –150 km s^{-1}), shallow (normalized intensity c. 0.9) absorption. Line core polarization remained above 1% and the blue wing polarization feature disappeared. The line core polarization maintained a largely (–%q, +%u; green diamonds) orientation in the qu-plot (see the post-eclipse binned epoch presented in Figure 2).

Clearly, the passage of the rotating, dark disk in front of the F star induces polarization signals away from line center. Continuing observations may be able to demonstrate whether the persistent line core polarization tracks the F star or a disk-tied source velocity around the orbit.

4.3. Hydrogen alpha linear polarization position angle

We calculated the position angle for (%q, %u) pairs for the H-alpha line in mid-eclipse (Figure 3). The data are rotated to the stellar frame and are not binned. Notice that the linear polarization position angle appears randomly scattered outside of the line, which is expected. The position angles that correspond to the line core (± 25 km s^{-1} from rest wavelength) are plotted in green; position angles corresponding to the blue-shifted absorption wing (–125 km s^{-1} to -25 km s^{-1}) are plotted in blue; and position angles corresponding to the red-shifted absorption wing (+25 km s-1 to +125 km s-1) are plotted in red. Position angles only range from 0° to 180° because of the nature of the Stokes parameters; a position angle of 180° is consistent with 0°. Notice the line core polarization is offset by about 90° from the wings. This may be an opacity effect. Compare these data to the mid-eclipse qu-plot (Figure 2).

4.4. Hydrogen beta

Unlike the pre-eclipse H-alpha line, the H-beta line (rest wavelength 486.135 nm) was better fitted by a Lorentzian profile and we adopted the HWHM of this profile (c. 35 km s^{-1}) as the line core. We further defined the wings as follows: the blue wing (–125 km s^{-1} to -35 km s^{-1}) and the red wing (35 km s^{-1} to 125 km s^{-1}) and noted that regions outside of the defined areas consistently mapped to (0,0) in the qu-plots. These definitions are maintained throughout the following analysis.

H-beta also exhibited persistent polarization in the line core in all epochs (see Figure 4). In pre-eclipse, the normalized intensity was at 13%, but the signal-to-noise remained above 1,000. The ratio p/σ was consistently greater

than 4 for %p greater than 0.22%. The –%q excursion in the qu-plot (Figure 5) corresponds to line core polarization and differs in orientation from H-alpha pre-eclipse (see Figure 2). The line itself appeared nearly symmetric and red-shifted by about the velocity of the F star at that phase.

The H-beta line maintained a deep and broad absorption at mid-eclipse that deepened further by late eclipse. %p increased in mid- and late eclipse. At mid-eclipse, the normalized intensity fell to about 5% at the deepest part of the line, but signal-to-noise remained greater than 500. The linear polarization was greatest at the line core, with smaller contributions from the blue and red absorption wings. The ratio p/σ remained consistently greater than 4 for %p $\geq$ 0.2% in this epoch. There were excursions in the qu-plot for features in the line core (–%q; green diamond), as well as the blue (+%q, +%u; blue square) and red (+%q, –%u; red triangle) absorption wings (Figure 5). These qu-plot excursions are similar to those exhibited by H-alpha for this epoch.

By late eclipse, the line exhibited a broad, deep, blue-shifted absorption. The line is clearly saturated in late eclipse, falling to just 1.6% intensity at the deepest point and, although S/N is nearly 200 here, the ratio p/σ is only 1.2; therefore %p = 0. The ratio p/σ ranged from 3 to 11 for %p > 0.4 outside the saturated region. The central core polarization appears to have decreased; the blue wing polarization (outside of the saturated region) increased (>2% at –70 km s^{-1}), while the red wing polarization decreased (c. 0.2% at 70 km s^{-1}) from mid-eclipse levels. In the qu-plot, the line core accounted for the –%q features ($p/\sigma \geq 3$ at –20 km s^{-1}; $p/\sigma \geq 4$ at –10 km s^{-1} and throughout the remainder of the core), the unsaturated blue wing accounted for the +%q features (Figure 5; blue squares) and the red wing polarization was largely concentrated at (0,0). The polarization behavior also followed the line behavior in this epoch and qualitatively resembles the H-alpha polarization.

The H-beta line did not return to its pre-eclipse form by the time of our last post-eclipse observation (January 17, 2012). The line was deeper, broader, and blue-shifted by about –20 km s^{-1} with a strong (c. 1.5%), narrow polarization peak centered on this velocity. The line was deep, but unsaturated, with normalized intensity nearly 8% and signal-to-noise above 500. The ratio p/σ remained above 4 for %p greater than 0.5%. The line core polarization maintained a largely –%q orientation in the qu-plot (see the post-eclipse binned epoch presented in Fig. 5).

4.5. Hydrogen gamma and Hydrogen delta

In pre-eclipse, H-gamma (rest wavelength 434.047 nm) appeared to exhibit low-level polarization features, but there were insufficient data points corresponding to $p/\sigma \geq 4$. H-delta (rest wavelength 410.008 nm) in pre-eclipse showed no polarization features. By mid-eclipse, both lines became saturated, making analysis of line core polarization impossible. However, both lines exhibited absorption wing polarization meeting the $p/\sigma \geq 4$ criteria.

These features exhibited excursions in the qu-plot of +%u for blue-shifted absorption and –%u for red-shifted absorption for both lines, which is consistent with both H-alpha and H-beta polarization during this epoch. The lines remained saturated in late eclipse and there were no significant polarization features post-eclipse for either line.

4.6. Potassium (769.896 nm)

The K I line (rest wavelength 769.896 nm) described here is the weaker line of a doublet that arises from the ground state. The out-of-eclipse line is thought to have an interstellar origin (Welty and Hobbs, 2001). The K I 769.896 nm line exhibited no polarization signatures until after mid-eclipse. We identified no F-star contribution; varying absorption and polarization features described below may be attributed to the disk.

In pre-eclipse, the line profile remained constant; the stellar radial velocity was red-shifted with respect to the line rest wavelength (see Figure 6); and no linear polarization features were observed (see examples, Figures 6 and 7). A Gaussian fit to the line profile returned a HWHM of 0.02 nm.

After first contact, the line exhibited a red-shifted (about 20 km s^{-1}) feature initially about the same depth as the line core (normalized intensity about 0.7) that deepened to a normalized intensity of about 0.3. There were no significant ($p/\sigma \geq 3$) polarization features evident until after second contact. The weak (c. 0.3%), narrow linear polarization feature that appeared after second contact was centered on the red-shifted component of the line.

By mid-eclipse the line appeared deeper and broader than during pre-eclipse epochs. A broad, weak (< 0.2%) linear polarization feature appeared which was centered on the line (see Figure 6). In Figure 6, the ratio p/σ is greater than 3 for polarization above 0.1% and is greater than 4 for polarization above 0.15%; the polarization is significant by Rice statistics. The stellar radial velocity was not shifted with respect to the line rest wavelength at mid-eclipse.

The line developed a broad, blue-shifted component after mid-eclipse. Polarization remained low (below 0.2%) until late eclipse, when the line was very broad. We fit a Gaussian function to the late eclipse line profile; the fit yielded a HWHM of 0.05 nm, more than twice the HWHM measured in pre-eclipse. The Gaussian centroid corresponded to a shift of –20 km s^{-1} from the rest wavelength. A larger (c. 0.5%) polarization feature was centered on the blue-shifted component of the line in this epoch (see Figure 6), which corresponded to a (–%q, +%u; blue squares) loop in the qu-plot (Figure 7). The star's radial velocity became blue-shifted with respect to the line rest wavelength after mid-eclipse.

The line retained a blue-shifted component after 4th contact that decreased in breadth and depth over time. There were no polarization features evident after 4th contact. The line had nearly returned to its pre-eclipse form by our last observation (January 17, 2012).

We examined the stronger line of the K I doublet, (rest wavelength 766.490 nm) and discovered that it exhibited line profile and polarization variations similar to the weaker line. At late eclipse, the line exhibited a broad, blue-shifted absorption component. A linear polarization feature was centered on the blue-shifted component and the qu-plot also exhibited a (–%q, +%u) loop.

4.7. Calcium (422.673 nm)

The Ca I line (rest wavelength 422.673 nm) described here arises from the ground state and shows a persistent core polarization signature in pre-, mid- and late eclipse phases (Figure 8). The late eclipse polarization appeared dramatically greater than the pre-eclipse phase. After first contact, the Ca I line exhibits variations similar to the K I line, with an additional absorption component at about +20 km s^{-1} from the line rest wavelength before mid-eclipse and a blue-shifted additional absorption component developing at about –20 km s^{-1} after mid-eclipse.

We fit the pre-eclipse Ca I line with a Gaussian function and adopted the HWHM of the Gaussian (36 km s^{-1}) as the line core. The Gaussian centroid was displaced from rest by 0.08 nm (24 km s^{-1}), but the calculated radial velocity of the star was only 8 km s^{-1} for this epoch. We confirmed the Gaussian HWHM using data for two later epochs (20081216, 20080213) when the Gaussian centroid and stellar radial velocity were more closely aligned. We defined the wings as follows: the blue wing (–125 km s^{-1} to –36 km s^{-1}) and the red wing (36 km s^{-1} to 125 km s^{-1}). Regions outside of these defined areas consistently mapped to (0,0) in the qu-plots. These definitions are maintained throughout the following analysis.

The line appeared asymmetric in the pre-eclipse epoch (Figure 8) with a red absorption component extending beyond the line core, at about 50 km s^{-1}. A large (c. 1%) polarization peak was nearly centered on the star and a smaller (0.4%) linear polarization peak was associated with the red-shifted component.

The presence of two peaks in %p for this pre-eclipse epoch may be attributed to one of the following: (1) the line is optically thick at the line core (as with H-alpha), (2) more than one asymmetric region contributes to the Ca I 422.6 nm polarization, or (3) the line contains a blend of species with varying degrees of polarization. Two species, Fe I (422.743 nm, 3.3 eV, doublet) and Ti II (422.733 nm, 1.13 eV, multiplet 33), are candidates for possible blended species corresponding to the velocity offset of c. 50 km s^{-1}. The possible blended feature persisted at about the same polarization strength throughout the time series. The corresponding Fe I doublet (422.545 nm) to our candidate line exhibited no polarization in any epoch. The two other members of the Ti II multiplet (421.818 nm and 420.592 nm) did not show polarization features. Hack (1959) identified a Ti II line of comparable energy to our candidate Ti II line (Ti II, 454.5 nm, 1.13 eV, multiplet 30) as a solely F star line. The feature

at c. 50 km s^{-1} may be a Ti II component attributable to the F star.

The qu-plot (Figure 9) describes two dominant position angles for the line in this pre-eclipse epoch; the excursion of (–%q, +%u; green diamonds) corresponds to the line core and the excursion (+%q; red triangles) corresponds to the red wing. The position angles corresponding to the excursions in the qu-plot differ by about 90 degrees.

The Ca I 422.6 nm line increased in %p by mid-eclipse (peak polarization >1% centered at the line rest wavelength. The polarization increased from mid- through the late eclipse and broadened on the blueward side as the blue absorption component appeared in the spectra.

The qu-plot (Figure 9) corresponding to mid-eclipse may be complicated by the presence of a possible blended line. The line core corresponds to (–%q, +%u; green diamonds), the excursion of (+%q, +%u; red triangles) corresponds to the red absorption wing (a possible blend) and the blue-shifted absorption corresponds to (–%q, –%u; blue squares). A similar scenario corresponds to the late eclipse qu-plot, with the notable exception that the degree of polarization has obviously increased for the line center at (–%q, +%u; green diamonds).

The %p decreased after 4th contact and the line returned to its pre-eclipse shape. The linear polarization exhibited two peaks in %p, one centered on the F star and the other offset from the F star velocity by about +50 km s^{-1}, centered on the presumed Ti II feature. The qu-plot (Figure 9) describes two dominant position angles for the line in post eclipse; the excursion of (–%q; green diamonds) corresponds to the line core and the excursion (+%q; red triangles) corresponds to the red wing.

We examined other Ca I lines to discover if the polarization behavior of the ground state transition was consistent with other energy transitions of this atomic species. Another Ca I line (rest wavelength 430.774 nm) arises from a higher energy level (1.9 eV) and exhibited similar line profile changes during eclipse, however, there were insufficient data points corresponding to $p/\sigma \geq 4$ to compare polarization changes of this line with changes observed in the ground state Ca I line. We observed no linear polarization signatures in other Ca I lines of comparable energy transition levels to the Ca I line at 430.774 nm.

The polarization behavior of this line suggests that Ca I (422.6 nm) traces polarization associated with the F star itself, as well as disk effects. Kim (2008) noted a 67-day out-of-eclipse light variation. We speculate that the F star polarization features we observed might be associated with upwelling and large scale bright convective regions.

4.8. Circular polarization and Stokes V

We identified no significant Stokes V (circular) polarization signal in any of the spectral lines we have described. Our preliminary assessment is that there are no significant circular polarization features in the data set. The presence of circular polarization signatures could indicate that magnetic fields are present

and contribute to polarization; the lack of signal suggests that magnetic fields are not a major contributor to the polarization we observed.

5. Results

The presence of persistent polarization in spectral lines such as H-alpha, H-beta, and the Ca I 422.6 nm line out-of-eclipse suggests that asymmetry persists in the F star for extended periods. H-alpha polarization was identified in ESPaDOnS observations of ε Aur dated February 7 and 8, 2006 (Harrington and Kuhn 2009), at phase 0.925, more than three years before the recent eclipse and about two years before periastron. Those observations, as well as the H-alpha observations presented here, indicated that the blue and red emission wings are not polarized, suggesting possible symmetry in the emitting region (at these shifted velocities/temperatures), or insufficient optical depth to generate detectable polarization from scattering in the region. We also observed that the H-alpha line does not saturate, unlike H-beta and others in the Balmer series. This suggests that a broad emission exists, contributing additional H-alpha photons to the line core.

We observed that H-alpha and H-beta exhibited different position angles in pre-eclipse. The H-beta absorption may indicate the presence of equatorially aligned hydrogen gas—the optically thick component scattering at 90 degrees perpendicular to the optically thin component. The H-alpha polarization position angles may include a component from interstellar polarization, or they may indicate a more complex distribution of hydrogen gas at those energies. Chadima *et al.* (2011) demonstrated that the atmosphere of the disk starts to be projected against the F star as early as three years before the beginning of the photometric eclipse; our observations seem to corroborate their findings.

H-alpha and H-beta showed similar mid- and late eclipse behavior in qu-space. The line cores and wings seem to agree about the range of angles involved, suggesting that the dominant features arise from the same orientation in the sky (gaseous material above and below the disk). An offset of 90 degrees between line core and absorption wings is consistent with the effect opacity may have on scattering.

The polarization behavior of the K I 769.9 nm line confirmed that this line has no F-star component; the line may be considered a bellwether for low excitation lines affected by the disk during eclipse. Limb polarization cannot be the sole contributor to polarization signatures during eclipse (for example, Kemp *et al.* 1986) because this line cannot have a limb polarization component. The disk exhibited significantly stronger polarization features in late eclipse than in any other eclipse epoch. Many observers have noted the asymmetry in the line (for example, Leadbeater *et al.* 2012). The increase in polarization may indicate that the density of scattering material increased in late eclipse. Pearson and Stencel (2012) note the "dawn" face of the disk may rotate into the

line-of-sight during late eclipse epochs. The warmed, presumably sublimated, material could contribute to the increased resonant scattering in the line. The position angles of scattering in late eclipse deviate from strict equatorial or polar alignment; modeling is required to replicate the late-eclipse Stokes %q and %u behavior.

The pre-eclipse polarization features of the Ca I 422.6 nm line showed contributions from the F star as well as from the eclipse. The increase in polarization in late eclipse is consistent with the K I line behavior and may also suggest an increase in the density of scattering material.

The spectral and linear polarization features presented here are a sample of the features present in the data set. Only a few epochs have been presented for brevity. We found significant changes to linear polarization in lines such as H-alpha, H-beta, Ca I 422.6 nm, and K I 796.6 nm presented here.

6. Conclusions and next steps

The analysis present here is a work in progress and is not a final word. There are many spectral features whose linear polarization characteristics remain to be described. We are optimistic about the potential in these data to help characterize polarization features that may be attributed to the F star itself, as well as the polarization that arises from the eclipsing disk. Our next steps in a subsequent paper will include identification and classification of spectral features that exhibit polarization, an analysis of the position angle of linear polarization features (to fully describe the linear polarization vector), and an analysis of scattering behavior when the F star is not uniformly eclipsed.

7. Acknowledgements

The authors are grateful for support of this work in part from a bequest in support of astronomy from the estate of William Herschel Womble. Based on observations obtained at the Canada-France-Hawaii Telescope (CFHT), which is operated by the National Research Council of Canada, the Institut National des Sciences de l'Univers of the Centre National de la Recherche Scientique of France, and the University of Hawaii. We would like to thank Roberto Casini, Elizabeth Griffin, Philip Judge, Brian Kloppenborg, Bruce Lites, and Jan Stenflo for helpful discussions.

The authors are very grateful to the referee, John Landstreet, for many helpful suggestions and improvements to the work.

References

Bagnulo, S., Landolfi, M., Landstreet, J.D., Landi Degl'Innocenti, E., Fossati, L., and Sterzik, M. 2009, *Publ. Astron. Soc. Pacific*, **121**, 993.
Chadima, P., *et al.* 2011, *Astron. Astrophys.*, **530**, 146.
Clarke, D. 2010, *Stellar Polarimetry*, Wiley-VCH, Hoboken, NJ.
Clarke, D., and Stewart, B. G. 1986, *Vistas Astron.*, **29**, 27.
Code, A., and Whitney, B. 1995, *Astrophys. J.*, **441**, 400.
Cole, G. 2012, *J. Amer. Assoc. Var. Star Obs.*, **40**, 787.
Coyne, G. 1972, *Ric. Astron.*, **8**, 311.
Donati, J.-F. 2003, in *Solar Polarization*, Eds. J. Trujillo-Bueno and J. Sanchez Almeida, ASP Conf. Proc., 307, Astron. Soc. Pacific, San Francisco, 41.
Donati, J.-F., Semel, M., Carter, B.D., Rees, D. E., and Collier Cameron, A. 1997, *Mon. Not. Roy. Astron. Soc.*, **291**, 658.
Hack, M. 1959, *Astrophys, J.*, **129**, 291.
Harrington, D., and Kuhn, J. 2009, *Astrophys. J., Suppl. Ser.*, **180**, 138.
Henson, G., Burdette, J., and Gray, S. 2012, in *Stellar Polarimetry: From Birth to Death*, AIP Conf. Proc. 1429, Amer. Inst. Physics, Melville, NY, 140.
Kemp, J. C., Henson, G. D., Kraus, D., Beardsley, I., Carroll, L., Ake, T., Simon, T., and Collins, G. 1986, *Astrophys. J., Lett. Ed.*, **300**, 11.
Kim, H. 2008, *J. Astron. Space Sci.*, **25**, 1.
Kloppenborg, B., *et al.* 2010, *Nature*, **464**, 870.
Leadbeater, R., *et al.* 2012, *J. Amer. Assoc. Var. Star Obs.*, **40**, 729.
Pearson, R. L., and Stencel, R. E. 2012, *J. Amer. Assoc. Var. Star Obs.*, **40**, 802.
Simmons, J. F., and Stewart, B. G. 1985, *Astron. Astrophys.*, **142**, 100.
Stefanik, R. P., Torres, G., Lovegrove, J., Pera, V. E., Latham, D. W., Zajac, J., and Mazeh, T. 2010, *Astron. J.*, **139**, 1254.
Stencel, R., *et al.* 2011 *Astron. J.*, **142**, 174.
Taylor, J. 1997, *Introduction to Error Analysis, the Study of Uncertainties in Physical Measurements*, 2nd Edition, University Science Books, New York.
Vaillancourt, J. 2006, *Publ. Astron. Soc. Pacific*, **118**, 1340.
Welty, D., and Hobbs, L. 2001, *Astrophys. J., Suppl. Ser.*, **133**, 345.

Table 1. Log of observations.

Comment[a]	*Gregorian*	*RJD*[b]	*Phase*[c]
	2006-01-07	3774.93	0.926
	2008-08-25	4704.04	0.019
	2008-10-18	4757.92	0.025
	2008-12-07[d]	4807.82	0.030
	2008-12-08[d]	4808.83	0.030
	2008-12-09[d]	4809.83	0.030
	2008-12-10[d]	4810.83	0.030
	2008-12-16	4817.05	0.031
	2009-02-13	4875.71	0.036
	2009-02-14	4876.70	0.037
	2009-02-17	4879.85	0.037
	2009-05-04	4955.72	0.045
1st contact	2009-08-22	5060	
	2009-09-04	5079.05	0.057
	2009-09-05	5080.07	0.057
	2009-09-08	5083.15	0.057
	2009-09-11	5086.11	0.058
	2009-09-25	5100.05	0.059
	2009-09-26	5101.02	0.059
	2009-09-29	5104.03	0.060
	2009-10-02	5107.02	0.060
	2009-10-07	5112.01	0.060
	2009-10-10	5115.16	0.061
	2009-11-29	5165.11	0.066
	2009-12-02	5168.00	0.066
	2009-12-04	5169.80	0.066
	2009-12-07	5173.14	0.067
	2009-12-08	5174.14	0.067
	2010-01-02	5198.77	0.069
2nd contact	2010-01-02	5200	
	2010-01-26	5222.71	0.072
	2010-01-28	5224.70	0.072
	2010-03-08	5263.72	0.076
mid-eclipse	2010-07-06	5390	
	2010-07-23	5401.12	0.090
	2010-08-01[d]	5410.13	0.090
	2010-08-05[d]	5414.11	0.091
	2010-10-16	5485.91	0.098
	2010-10-18	5487.90	0.098
	2010-10-19	5488.99	0.098

Table continued on next page

Table 1. Log of observations, cont.

Comment[a]	*Gregorian*	*RJD*[b]	*Phase*[c]
	2010-10-21	5490.93	0.099
	2010-11-15	5516.02	0.101
	2010-11-16	5517.14	0.101
	2010-11-17	5517.96	0.101
	2010-11-22[d]	5522.89	0.102
	2010-11-24[d]	5524.99	0.102
	2010-12-19	5549.74	0.105
3rd contact	2011-03-18	5620	
4th contact	2011-05-21	5720	
	2011-08-17	5791.13	0.129
	2011-11-01	5867.13	0.137
	2011-11-15d	5880.99	0.138
	2011-11-16d	5882.16	0.138
	2012-01-06	5933.00	0.143
	2012-01-17	5943.78	0.144

Notes: [a]RJD for eclipse taken from Stencel et al. *(2011); [b]Julian date—2450000; [c]Time of periastron and period from Stefanik* et al. *(2010) 2434723+9896.0E; [d]Epoch binning as follows: early—binned 20081207, 20081208, 20081209, 20081210; mid—binned 20100801 and 20100805; late—binned 201122 and 20111124; post—binned 20111115, 2011116.*

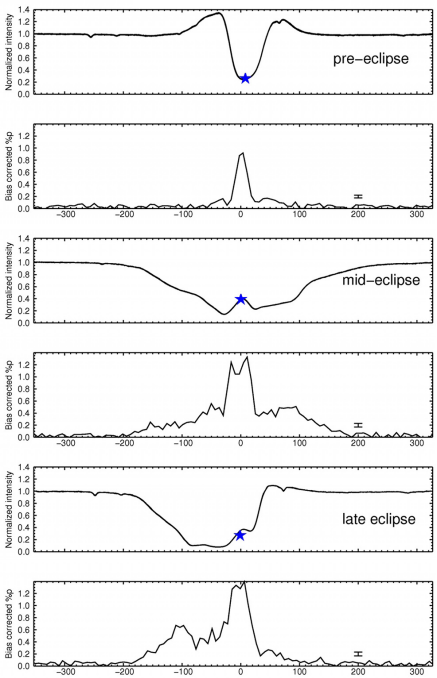

Figure 1. Time series of H-alpha (656.280 nm) line and %p profiles for pre-, mid-, and late-eclipse epochs. Velocity is centered on the line rest wavelength. The F-star radial velocity is indicated by a star symbol. Note the star is slightly red-shifted pre-eclipse and blue-shifted late eclipse. Polarization data are epoch- (see text) and wavelength-binned (bin size 0.015 nm). Average errors in %p are shown.

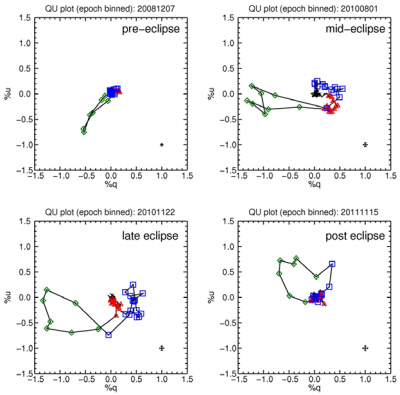

Figure 2. QU-plots of H-alpha (656.280 nm) for pre-, mid-, late, and post-eclipse epoch and wavelength binned data. The first date of each binned epoch is given. Average error bars are shown. Note the QU-plot is nearly linear in pre-eclipse. The prominent excursion (–%q, –%u; green diamonds) corresponds to the line core (± 25 km s^{-1}). Absorption wing contributions appear in mid- and late-eclipse. The blue wing corresponds to (+%q, +%u; blue squares) and the red wing corresponds to (+%q, –%u; red triangles) in mid-eclipse. By late eclipse, the red wing polarization has largely disappeared (near 0,0) and the large +%q excursion is blue wing polarization. The line core polarization is (+%u, –%q; green diamonds) in post eclipse. These data have been rotated into the stellar frame (see text for description).

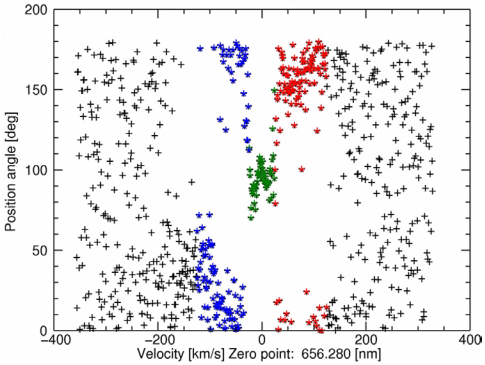

Figure 3. Position angle calculated for (%q, %u) pairs for the H-alpha line in mid-eclipse. The data are rotated to the stellar frame and unbinned. Notice that the linear polarization position angle appears randomly scattered outside of the line, which is expected. The position angles that correspond to the line core (± 25 km s^{-1} from rest wavelength) are plotted in green; position angles corresponding to the blue-shifted absorption wing (–125 km s^{-1} to –25 km s^{-1}) are plotted as blue star-shapes; and position angles corresponding to the red-shifted absorption wing (+25 km s^{-1} to +125 km s^{-1}) are plotted as red star-shapes. Position angles only range from 0° to 180° because of the nature of the Stokes parameters; a position angle of 180° is consistent with 0°. Notice the line core polarization is offset by about 90° from the wings. This may be an opacity effect. Compare these data to the mid-eclipse QU-plot (Figure 2) and mid-eclipse line profile (Figure 1).

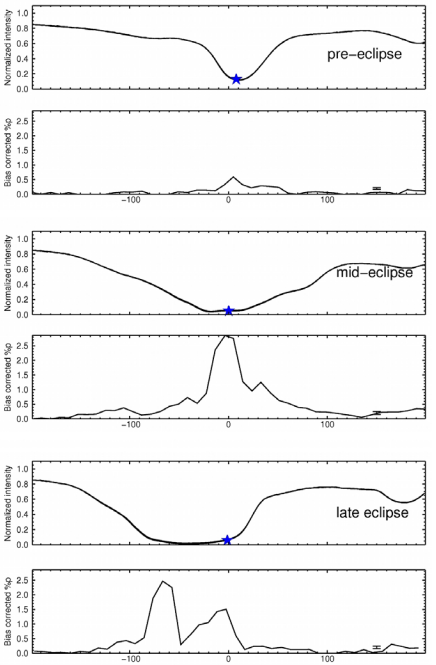

Figure 4. Time series of H-beta (486.135 nm) line and %p profiles for pre-, mid-, and late-eclipse epochs. Velocity is centered on the line rest wavelength. The F-star radial velocity is indicated by a star symbol. Polarization data are epoch- (see text) and wavelength binned (bin size 0.015 nm). Average errors in %p are shown. The line is clearly saturated in late eclipse, falling to just 1.6% intensity at the deepest point and, although S/N is nearly 200 here, the ratio p/σ is only 1.2; therefore %p = 0. The ratio p/σ ranges from 3 to 11 for %p > 0.4 outside the saturated region.

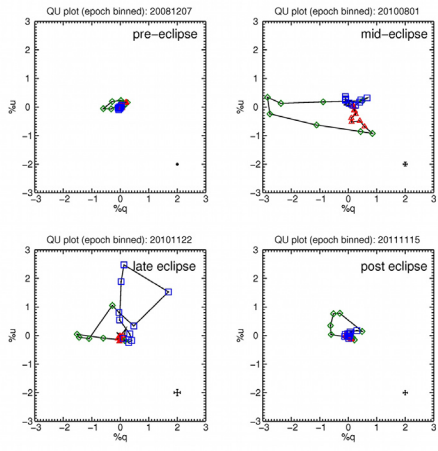

Figure 5. QU-plots of H-beta (486.135 nm) for pre-, mid-, late-, and post-eclipse epoch- and wavelength-binned data. The first date of each binned epoch is given. Average error bars are shown. Absorption wing contributions appear in mid- and late-eclipse. The blue wing corresponds to (+%q, +%u; blue squares) and the red wing corresponds to (+%q, –%u; red triangles) in mid-eclipse. Line core is –%q (green diamonds). By late eclipse, the red wing polarization has disappeared (centered on 0,0) and the large +%q excursion is blue wing polarization (blue squares). The line core polarization is +%u in post eclipse. These data have been rotated into the stellar frame (see text for description).

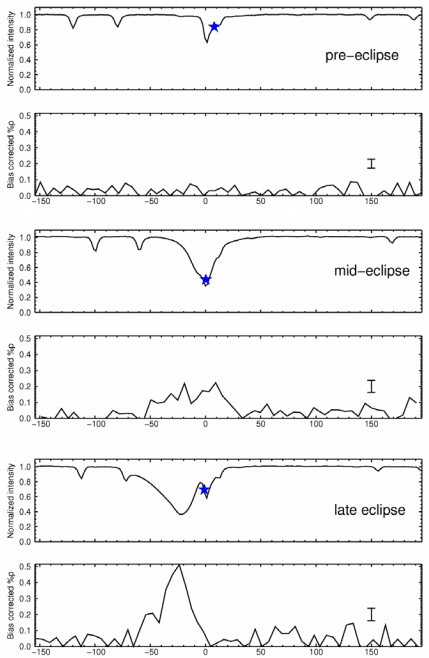

Figure 6. Time series of a K I (769.896 nm) line and %p profiles for pre-, mid-, and late-eclipse epochs. Velocity is centered on rest wavelength. Polarization data are epoch- (see text) and wavelength-binned (bin size 0.015 nm). The out-of-eclipse line is thought to have an interstellar origin. Note the star is red-shifted pre-eclipse, but the line core is not red-shifted and the line exhibits no polarization features. Disk contributions to the line in late eclipse are blue-shifted and exhibit polarization features.

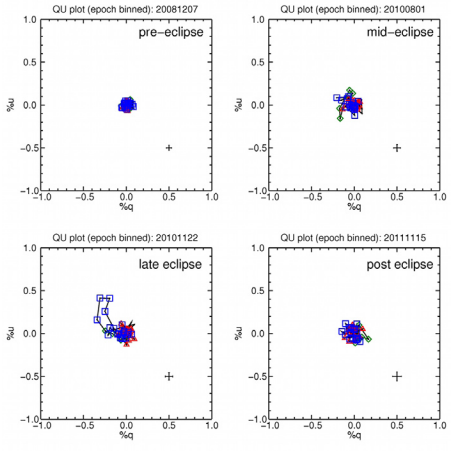

Figure 7. QU-plots of K I (769.896 nm) for pre-, mid-, late-, and post-eclipse epoch- and wavelength-binned data. The first date of each binned epoch is given. Average error bars are given. The out-of-eclipse line is thought to have an interstellar origin (for example, Welty and Hobbs, 2001). Note there are no polarization features pre-eclipse or post eclipse. Disk contributions appear after mid-eclipse. The (–%q, +%u; blue squares) excursion corresponds to the blue-shifted absorption wing. These data have been rotated into the stellar frame (see text for description).

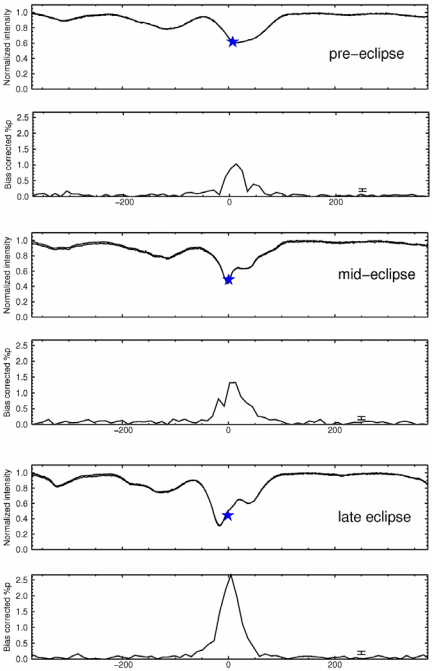

Figure 8. Time series of a Ca I (422.673 nm) line and %p for pre-, mid-, and late-eclipse epochs. Velocity is centered on the line rest wavelength. This line corresponds to a ground state transition. Note the dramatic increase in linear polarization in later epochs. The data are epoch- (see text) and wavelength-binned (bin size 0.015 nm). Average errors in %p are shown.

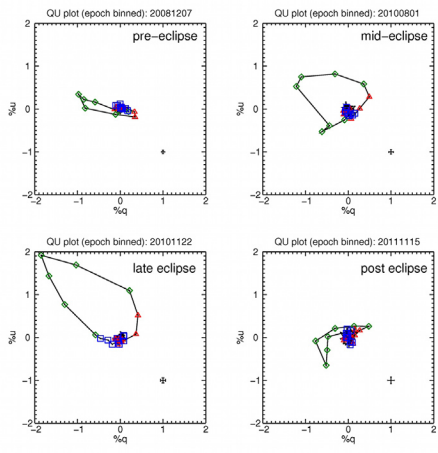

Figure 9. QU-plots of Ca I (422.673 nm) for pre-, mid-, late-, and post-eclipse epoch- and wavelength-binned data. The first date of each binned epoch is given. Average error bars are shown. Absorption wing contributions appear in mid- and late-eclipse. The QU-loop (green diamonds) largely corresponds to line core, with small red wing contributions in +%q in mid-eclipse (red triangles). By late-eclipse, the QU-loop has grown with small –%q contributions from the blue wing (blue squares) and +%q contributions from the red wing. The "flattened" QU-loop corresponds to line core (green diamonds) in post eclipse. These data have been rotated into the stellar frame (see text for description).